Energy and Electron Transfer Dynamics within a Series of Perylene Diimide/Cyclophane Systems

Seán T. J. Ryan,[†] Ryan M. Young,[‡,¶] James J. Henkelis,[‡] Nema Hafezi,[‡] Nicolaas A. Vermeulen,[‡] Andreas Hennig,[§] Edward J. Dale,[‡] Yilei Wu,[‡,¶] Matthew D. Krzyaniak,[‡,¶] Athan Fox,[†] Werner M. Nau,[§] Michael R. Wasielewski,[‡,¶] J. Fraser Stoddart,[‡] and Oren A. Scherman[*,†]

Melville Laboratory for Polymer Synthesis, Department of Chemistry, University of Cambridge, Lensfield Road, Cambridge, CB2 1EW, U.K., Department of Chemistry, Northwestern University, Evanston, Illinois 60208-3113, United States, Argonne-Northwestern Solar Energy Research (ANSER) Center, Northwestern University, Evanston, Illinois 60208-3113, United States, and School of Engineering and Science, Jacobs University Bremen, Campus Ring 1, 28759 Bremen, Germany

E-mail: oas23@cam.ac.uk

[*]To whom correspondence should be addressed

[†]Melville Laboratory for Polymer Synthesis, Department of Chemistry, University of Cambridge, Lensfield Road, Cambridge, CB2 1EW, U.K.

[‡]Department of Chemistry, Northwestern University, Evanston, Illinois 60208-3113, United States

[¶]Argonne-Northwestern Solar Energy Research (ANSER) Center, Northwestern University, Evanston, Illinois 60208-3113, United States

[§]School of Engineering and Science, Jacobs University Bremen, Campus Ring 1, 28759 Bremen, Germany

Abstract

Artificial photosynthetic systems for solar energy conversion exploit both covalent and supramolecular chemistry to produce favorable arrangements of light-harvesting and redox-active chromophores in space. An understanding of the interplay between key processes for photosynthesis, namely light-harvesting, energy transfer, and photoinduced charge separation and the design of novel, self-assembling components capable of these processes are imperative for the realization of multifunctional integrated systems. We report our investigations on the potential of extended tetracationic cyclophane/perylene diimide systems as components for artificial photosynthetic applications. We show how the selection of appropriate heterocycles, as extending units, allows for tuning of the electron accumulation and photophysical properties of the extended tetracationic cyclophanes. Spectroscopic techniques confirm energy transfer between the extended tetracationic cyclophanes and perylene diimide is ultrafast and quantitative, while the heterocycle specifically influences the energy transfer related parameters and the acceptor excited state.

Introduction

The recently synthesized, extended tetracationic cyclophane,[1] **ExBox**$^{4+}$, comprising two phenylene-extended bipyridinium units linked together by two *p*-xylylene (*p*-Xy) bridges to form a rectangular macrocycle, has received attention on account of its potential for inclusion in artificial photosynthetic systems. Numerous properties render **ExBox**$^{4+}$ an attractive candidate for such applications, including ultrafast, intermolecular charge transfer from a suitable electron-rich guest,[2] intramolecular through-bond charge transfer from the *p*-Xy bridges to the extended bipyridinium units[3] (ExBIPY^{2+}) and multi-electron accumulation[1,3] leading to an array of accessible mixed-valence states. Most recently, we reported[4] the first incidence of energy transfer (EnT), an essential process of all biological photosynthetic systems,[5–10] within the extended tetracationic cyclophane (Ex^{1}Box) family. The discovery of

EnT within Ex^1Box systems opens up new possibilities for greater complexity and biomimetic function with regard to their inclusion in switchable, photoactive, mechanically interlocked systems[11,12] and light-harvesting arrays for device applications.[13–15]

Perylene diimides (PDIs) have received much attention for their high thermal, chemical, electrochemical and photophysical stability.[13] Recent studies have found particular suitability of this highly versatile family of compounds in applications such as organic photocatalysis[16] and solar water splitting,[17,18] one of the most important photosynthetic processes due to its potential to provide a large scale, clean source of carbon-free energy.[19]

We develop our understanding of the viability of combined Ex^1Box/PDI systems to act as components in artificial photosynthetic systems, on account of their electron-accumulation and light-harvesting properties.

In order to comprehensively characterize the Ex^1Box/PDI systems, we synthesized three series of $ExBIPY^{2+}$ species. Firstly, the extended methyl viologens[20] (MExVs) where phenylene, thiophene and selenophene are used as the extending units to yield $\mathbf{MPV}^{2+}$, $\mathbf{MTV}^{2+}$ and $\mathbf{MSeV}^{2+}$, respectively (as shown in the ESI). The MExVs serve as controls for the second series, the Ex^1Boxes, the corresponding members of which are $\mathbf{ExBox}^{4+}$, $\mathbf{TExBox}^{4+}$ and $\mathbf{SeExBox}^{4+}$ (Figure 1). The third series further increases the complexity of the $ExBIPY^{2+}$ chemical environment *via* complexation and subsequent catenation[21,22] of the Ex^1Boxes with a dicationic PDI derivative. The three Ex^1Box/PDI [2]catenanes (ExCats) are designated $\mathbf{ExCat}^{6+}$, $\mathbf{TExCat}^{6+}$ and $\mathbf{SeExCat}^{6+}$ (Figure 2).

Results and discussion

Synthesis and Structural characterization

The MExVs, $\mathbf{MTV}^{2+}$ and $\mathbf{MSeV}^{2+}$, and Ex^1Boxes, $\mathbf{TExBox}^{4+}$ and $\mathbf{SeExBox}^{4+}$, were synthesized *via* analogous protocols[1] to $\mathbf{MPV}^{2+}$ and $\mathbf{ExBox}^{4+}$ (as detailed in the ESI). $\mathbf{TExBox}^{4+}$ and $\mathbf{SeExBox}^{4+}$ were obtained in yields of 37 % and 44 %, respectively, which

are significantly higher than the non-templated yield reported[1] for $\mathbf{ExBox}^{4+}$ (19 %), presumably on account of the reduced symmetry of $\mathbf{TExBox}^{4+}$ and $\mathbf{SeExBox}^{4+}$, which induces lower bond angle strain in the transition state of the ring closing reaction. The ^{1}H NMR spectra of the Ex^{1}Boxes and their corresponding X-ray crystal structures are shown in Figures 1 and S1.

The Hay modification of the terminal alkyne Glaser homocoupling reaction[23,24] in aqueous media was selected for the catenation procedure[25] (Figure 2) as complexation between the Ex^{1}Boxes and **PDI-E1** was observed only in water and not in organic solvents (Figures S2-S4). Binding constants on the order of 10^4 M^{-1} were obtained by isothermal titration calorimetry (Figure S7). The reaction conditions employed consisted of an aerated aqueous solution of **PDI-E2** (1 mM), three equivalents of Ex^{1}Box host and excesses of CuCl and tetramethylethylenediamine, stirred at 30 °C. Upon completion (monitored by analytical HPLC), the reaction mixture was centrifuged to remove the solid copper residue. The supernatant was subjected to reverse phase column chromatography and the fractions containing pure product, analyzed by analytical HPLC, were combined and lyophilized. The trifluoroacetate counterions were then exchanged for chloride counterions using tetrabutylammonium chloride (NBu_4Cl).

The catenanes, $\mathbf{ExCat}^{6+}$, $\mathbf{TExCat}^{6+}$ and $\mathbf{SeExCat}^{6+}$ were obtained in yields of 19%, 14% and 16%, respectively. ^{1}H NMR of the ExCats revealed shifts in the resonances associated with the Ex^{1}Box components nearly identical to those identified as complexed peaks *via* titrations (Figures 2, S2-S3, S5), while DOSY NMR revealed that both PDI and Ex^{1}Box components diffuse at equal rates (Figure S6). X-ray crystallography also confirmed the acquisition of the target compounds,[26] which reveal closely-packed extended superstructures supported by an extensive network of C-H – F interactions between the aromatic hydrogen atoms of the Ex^{1}Boxes and fluorine atoms of the PF_6^- counterions (Figures S8-S9).

Electrochemical Characterization

Cyclic voltammetry (CV) of the MExVs, Ex^{1}Boxes and ExCats was performed in dimethyl sulfoxide (Me_2SO) at a concentration of 1 mM with a sweep rate of 50 mV s^{-1} against a Ag/AgCl reference electrode. All redox couple potentials are summarized in Table 1. CV (Figure S10) reveals that each of the MExVs undergo two one-electron reductions. **MPV**$^{2+}$ possesses the most negative reduction potential, which is smooth and non-broadened, indicating little or no communication between the two pyridinium centers. **MSeV**$^{2+}$ and **MTV**$^{2+}$ posses more positive reduction potentials with small and significant shouldering, respectively, demonstrating progressively higher levels of communication.

Upon incorporation of the ExBIPY^{2+} units into the Ex^{1}Boxes, their redox properties are significantly altered (Figure S11). **ExBox**$^{4+}$ reveals two overlapping two-electron reduction peaks without any obvious shouldering. The degree of communication within **ExBox**$^{4+}$ in Me_2SO is significantly lower than that found in dimethylformamide[1] (DMF). **TExBox**$^{4+}$ and **SeExBox**$^{4+}$, in line with the previous trend, display more positive reduction potentials. There is also significantly greater separation of the two two-electron redox couples, indicating greater communication within **TExBox**$^{4+}$ and **SeExBox**$^{4+}$, which is attributed to higher conformational restriction of their constituent aromatic rings, on account of the lower symmetry of their extending units. A close examination of the X-ray crystal structures of the Ex^{1}Boxes supports the notion that their relative conformations in the solution phase and solid state are similar.

Cyclic voltammograms of the ExCats exhibit three distinct redox couples (Figure S12). The first two represent the first and second one-electron reductions of the PDI component. The ExCats also exhibit a third redox couple with a much higher peak current than the first two reduction events, which represents the four one-electron reductions of the Ex^{1}Box components. This is likely on account of structural distortion of the Ex^{1}Boxes by the PDI guest, which eliminates any communication between the pyridinium units, thus facilitating their simultaneous reduction. As such, the Ex^{1}Box redox couples are smooth and non-

broadened. Thus, CV illustrates how all ExCats are capable of incrementally accepting up to six electrons, with tuneable reduction potentials over a range of 570 mV (-210 – -780 mV), where the PDI component's reduction potential may be altered over 270 mV (-210 – -480 mV). The reversibility of the redox peaks illustrates good electrochemical stability at a 50 mV s^{-1} scan rate.[27] The accessibility of various, stable mixed valence redox states is an essential property of artificial photosynthetic reaction centers, where the build up of charge enables the realization of multi-electron processes such as water splitting.[28–30]

Steady-state Photophysical Characterization

Having investigated the structural and electrochemical properties of the three series, we moved onto their photophysical properties in water. Steady-state electronic absorption and fluorescence emission studies (Figure 3) show that $\mathbf{MPV}^{2+}$ and $\mathbf{ExBox}^{4+}$ possess the highest singlet excitation energy ($^1{}^*E_S$) in their respective series, while $\mathbf{MSeV}^{2+}$ and $\mathbf{SeExBox}^{4+}$ possess the lowest. $\mathbf{MTV}^{2+}$ and $\mathbf{TExBox}^{4+}$ displayed the highest fluorescence quantum yields (Φ_f, 0.77 and 0.37, respectively), while $\mathbf{MSeV}^{2+}$ and $\mathbf{SeExBox}^{4+}$ displayed the lowest (0.0017 and 0.0027, respectively). The electronic absorption maxima show negligible shifting between the respective members of the MExV and Ex^1Box series. However, the fluorescence emission maxima of the Ex^1Boxes are all redshifted relative to the MExVs. As such, the $^1{}^*E_S$ of the Ex^1Boxes are approximately 0.08 eV lower than their respective MExVs. The above parameters are detailed in Table 2.

The steady-state electronic absorption and fluorescence emission spectra of the ExCats in water are shown in Figure 4. An essential property of any solar energy conversion device is the ability to absorb light within the solar spectrum as measured at the earth's surface.[31] The spectral excitation window of $\mathbf{ExBox}^{4+}$ within $\mathbf{ExCat}^{6+}$, defined by the full width half maximum of the electronic absorption profile, lies outside the visible spectrum. However, the lower HOMO-LUMO gap of $\mathbf{TExBox}^{4+}$ and $\mathbf{SeExBox}^{4+}$ within their corresponding ExCats, induced by the more electron rich 5-membered heterocycles, leads to an overlap

of their excitation windows with the visible part of the solar spectrum. Thus, the light-harvesting properties of the Ex^{1}Boxes may be tuned by changing the identity of the extending unit and in conjunction with the PDI component, the ExCats are able to absorb over most of the solar spectrum. The excitation windows of the Ex^{1}Boxes within the ExCats are detailed in Table 4.

Lastly, the fluorescence excitation spectra of the ExCats (Figure 4, λ_{mon} = 550 nm) bear very strong similarity to their corresponding absorption spectra within the absorption region of the Ex^{1}Box components, clearly illustrating the EnT process active between the ExBIPY^{2+} and PDI chromophores.

Time-resolved Photophysical Characterization

Time-resolved photophysical experiments were next carried out in water to gain a greater insight into the excited state dynamics of the Ex^{1}Boxes and EnT dynamics of the ExCats. All excited state relaxation time constants are detailed in Table 3.

Firstly, the MExVs were investigated by femtosecond transient absorption (fsTA). We do not observe ground state bleaching of the MExVs or Ex^{1}Boxes due to a combination of the strong, overlapping absorption of the transient species with the ground state absorption and the 430 nm edge of the probe window. $\mathbf{MPV}^{2+}$, $\mathbf{MTV}^{2+}$ and $\mathbf{MSeV}^{2+}$ were excited at 330, 414 and 414 nm, respectively, with 150 fs pulses. Upon excitation of $\mathbf{MPV}^{2+}$, the first excited singlet state, ^{1}***MPV**$^{2+}$, is produced, which decays with an effective lifetime, τ_{eff} = 1330 ± 15 ps, by fluorescence to the ground state, $^0\mathbf{MPV}^{2+}$ (Figures S13-S14). Time-correlated single photon counting (TCSPC) recorded a similar lifetime of τ_{eff} = 1.40 ns (Figure S35). Spin-orbit intersystem crossing (SO-ISC) affords a minor contribution to the decay, producing the first excited triplet state, ^{3}***MPV**$^{2+}$, whose decay persists beyond 7 ns, the experimental time scale of our fsTA setup. Indeed, all triplet states investigated below persisted beyond this time scale.

^{1}***MTV**$^{2+}$ decayed in τ_{eff} = 1080 ± 8 ps by fsTA (Figures S13, S15), while TCSPC

recorded a slightly longer lifetime of τ_{eff} = 1.85 ns (Figure S35). SO-ISC again affords a small contribution decay, yielding ^{3}***MTV**$^{2+}$.

MSeV^{2+} displayed markedly different behavior (Figures S13, S16). ^{1}***MSeV**$^{2+}$ decayed rapidly *via* SO-ISC to produce ^{3}***MSeV**$^{2+}$ in τ_{eff} = 5.1 ± 0.1 ps. The almost exclusive contribution of SO-ISC to the decay kinetics[32] is attributed to the internal heavy atom effect[33] facilitated by the selenium atom, which also manifests in the Φ_f of **MSeV**$^{2+}$ (see Table 2).

The Ex^{1}Boxes were then investigated under the same conditions used for the MExVs (Figures 5, S17). A schematic illustration of the excited state dynamics of all Ex^{1}Boxes in water is shown in Scheme 1.

The initial fsTA spectrum of **TExBox**$^{4+}$ is characterized by absorptions at 482, 734, 1081 and 1246 nm, which are assigned to ^{1}***TExBox**$^{4+}$ (Figure S19), which decays *via* two parallel pathways in τ_{eff} = 447 ± 4 ps. The first pathway is *via* fluorescence to ^{0}**TExBox**$^{4+}$ (Figure 3), the lifetime of which (τ_f) may be estimated by the effective lifetime of ^{1}***MTV**$^{2+}$. The second pathway is the intramolecular, through-bond reduction of ExBIPY^{2+} by the *p*-Xy bridge, resulting in a photoinduced charge separated state,[3] TExBIPY^{+}-*p*-Xy^{+}, in a time, τ_{PCS}, characterized by absorbances at 576, 918 and 1065 nm.

$$\frac{1}{\tau_{eff}} = \frac{1}{\tau_f} + \frac{1}{\tau_{PCS}} \tag{1}$$

The relation between τ_{eff}, τ_f and τ_{PCS} is given by Equation 1. Thus, the approximation, $\tau_{PCS} \approx$ 763 ps, may be calculated. Visible-infrared spectroelectrochemistry corroborated the TExBIPY^{+}-*p*-Xy^{+} assignment. The spectrum reveals maxima at 578, 924 and 1066 nm (Figure S37), which is nearly identical to the reconstituted fsTA spectrum. The approximate free energy of photoinduced charge separation (PCS), ΔG_{PCS}, defined as the difference between the Ex^{1}Box singlet energy (see Table 2), and the ion pair energy of the photoinduced charge separated state, ΔG_{IP} (see Equation 2) was then calculated.

$$\Delta G_{PCS} = \Delta G_{IP} - {}^{1*}E \tag{2}$$

$$\Delta G_{IP} = E_{ox} - E_{red} + \Delta U + \Delta G_{solv} \tag{3}$$

ΔG_{IP} may be calculated by the equation developed by Weller[34] (Equation 3). E_{ox} is the oxidation potential of the *p*-Xy bridge (1.98 V vs. Ag/AgCl),[35] and E_{red} is the first reduction potential of the ExBIPY^{2+} unit, here taken as the first reduction potential of the corresponding MExV (see Table 1). ΔU, a coulombic correction factor, may be neglected as it has been shown to be small in **ExBox**$^{4+}$ in polar media.[3] ΔG_{solv}, a solvent correction factor, may also be neglected on account of the high dielectric constants of water and Me_2SO. Thus, in the case of **TExBox**$^{4+}$, ΔG_{PCS} is found to be approximately -0.31 eV, illustrating that PCS is an energetically downhill and spontaneous process.

Charge recombination then occurs in $\tau_{CR} = 2850 \pm 60$ ps, resulting in the formation of ^{3}***TExBox**$^{4+}$, *via* spin-orbit charge transfer intersystem crossing[36] (SOCT-ISC), on account of the favorable perpendicular orientation of the ExBIPY^{2+} and *p*-Xy chromophores, characterized by absorbances at 576, 914 and 1062 nm. The quantum yield for the formation of ^{3}***TExBox**$^{4+}$ in solution is unknown, as charge recombination to ^{0}**TExBox**$^{4+}$ likely occurs in parallel with SOCT-ISC.

^{3}***TExBox**$^{4+}$ was then investigated in the solid state *via* phosphorescence emission spectroscopy (PES, Me_2SO, 77 K, Figure S38), which displayed an emission signal with a maximum at 614 nm, giving a triplet energy ($^{1*}E_T$) of 2.02 eV. Time-resolved phosphorescence emission spectroscopy (TRPES, Me_2SO, 77 K, $\lambda_{mon} = 614$ nm) revealed a solid state lifetime of $\tau_p = 10.6$ ms, which is typical for organic compounds under such conditions.[37]

The fsTA spectrum[38] of ^{1}***SeExBox**$^{4+}$ is characterized by four absorbances at 497, 758, 1160 and 1309 nm. ^{1}***SeExBox**$^{4+}$ is very short lived, decaying in $\tau_{eff} = 6.6 \pm 0.1$ ps, principally *via* SO-ISC to ^{3}***SeExBox**$^{4+}$, characterized by absorptions at 475, 890 and 1027 nm. This singlet lifetime is very similar to that of ^{1}***MSeV**$^{2+}$, while the Φ_f of **SeExBox**$^{4+}$ (see

Table 2) demonstrates that fluorescence contributes negligibly to singlet decay. Relaxation of ^{3}***SeExBox**$^{4+}$ occurs in $\tau_{eff} = 2280 \pm 870$ ps. Based on the spectral similarities of the 2 ns component (Figures 5, S20) to ^{3}***SeExBox**$^{4+}$, it is attributed to triplet-triplet annihilation arising from collisional deactivation of ^{3}***SeExBox**$^{4+}$ with either another ^{3}***SeExBox**$^{4+}$ species or triplet oxygen (solutions were not deoxygenated prior to the laser experiments). Residual ^{3}***SeExBox**$^{4+}$ persists beyond 7 ns. The high efficiency of SO-ISC means that it kinetically outcompetes PCS. As such, despite the negative ΔG_{PCS} for **SeExBox**$^{4+}$ (approximately -0.35 eV), no evidence for SeExBIPY^{+}-*p*-Xy^{+} (Figure S37) was observed in the fsTA spectra. ^{3}***SeExBox**$^{4+}$ was further probed using nanosecond transient absorption (nsTA, Figures S31-S32), which revealed a short triplet lifetime of $\tau_{eff} = 2.80 \pm 0.01$ μs in oxygenated solution at room temperature.

PES (Me_2SO, 77 K) revealed a signal with a peak maximum at 640 nm, yielding a $^{1}*E_T$ of 1.94 eV (Figure S38). TRPES ($\lambda_{mon} = 640$ nm) revealed a triplet lifetime of $\tau_p = 0.2$ ms, which is two orders of magnitude greater than that measured using nsTA. Although fairly typical for organic phosphorescent compounds, this lifetime is still relatively short given the efficiency of triplet formation, which is likely on account of the internal heavy atom effect, which increases the rate of SO-ISC from ^{3}***SeExBox**$^{4+}$ to ^{0}**SeExBox**$^{4+}$.

Although already documented in organic media,[3] we repeated our studies of the excited state dynamics of **ExBox**$^{4+}$ in water. Upon excitation, ^{1}***ExBox**$^{4+}$ is produced, characterized by a single, intense absorbance at 499 nm, very similar to that observed in MeCN,[3] and a rising absorbance into the NIR region, which undergoes initial relation in $\tau_r = 73 \pm 1$ ps. ^{1}***ExBox**$^{+4}$ decays further in $\tau_{eff} = 413 \pm 10$ ps, and is replaced by a ^{3}***ExBox**$^{4+}$, characterized by a single peak at 490 nm. Interestingly, evolution of ExBIPY^{+}-*p*-Xy^{+}, previously observed upon decay of ^{1}***ExBox**$^{4+}$ in MeCN and characterized by a broad 900-1200 nm absorbance, is not observed in water.

The absence of an observed ExBIPY^{+}-*p*-Xy^{+} state was an unexpected result given the strong driving force for PCS.[3] As the decay of ^{1}***ExBox**$^{4+}$ is approximately three times

shorter than that of ^{1}***MPV**$^{2+}$, it is unlikely that ^{1}***ExBox**$^{4+}$ decays directly to ^{0}**ExBox**$^{4+}$ and ^{3}***ExBox**$^{4+}$. Inverted reaction kinetics, whereby the formation of the ExBIPY^{+}-*p*-Xy^{+} state is much slower than its decay *via* charge recombination, is the most likely explanation. A simplified analysis of the kinetics of charge recombination, using Marcus-Hush theory (see ESI), shows that the rate is approximately thirteen times faster in water than in MeCN. Using Equation 1 and the lifetime of ^{1}***MPV**$^{2+}$ as an approximation for τ_f, one may postulate $\tau_{PCS} \approx 599$ ps for ^{1}***ExBox**$^{4+}$, which is similar to that calculated for ^{1}***TExBox**$^{4+}$.

PES (Me_2SO, 77 K) revealed an **ExBox**$^{4+}$ triplet energy of 2.14 eV, while TRPES ($\lambda_{mon} = 515$ nm) was best fitted using a biexponential function with time constants $\tau_{p1} = 0.29$ s (26 %) and $\tau_{p2} = 0.94$ s (74 %). The approximate one second phosphorescence lifetime of ^{3}***ExBox**$^{4+}$ is on the long end of the scale for organic molecules.[39–41]

Having characterized the relaxation dynamics of the Ex^{1}Boxes, we turned our attention to the energy transfer dynamics of the ExCats. Investigations by fsTA were conducted using pump pulse wavelengths that selectively excite the Ex^{1}Box donors (Figures 6, S21). Schematic descriptions of the ExCat relaxation dynamics are shown in Scheme 2.

In all cases, the first excited singlet states of the Ex^{1}Box donors were not observed at all upon photoexcitation (Figures S22-S24), indicating excited state deactivation occurs within the 250 fs response time of the instrument. We can, therefore, conclude that the excited singlet states of the Ex^{1}Boxes within the three ExCats have lifetimes of less than 250 fs.

$$\eta = \frac{1}{1 + \tau'/\tau} \tag{4}$$

Equation 4 (τ = deactivation lifetime of the donor by all pathways in the absence of the acceptor (measured by fsTA above, see Table 3), τ' = lifetime of the energy transfer process between donor and acceptor) may then be used to calculate the EnT efficiency (η) between PDI and the three Ex^{1}Boxes. Taking τ' to be less than 250 fs, η is found to be greater than 99.99 % for **ExCat**$^{6+}$ and **TExCat**$^{6+}$, demonstrating that EnT is quantitative. In the case of **SeExCat**$^{6+}$, η is found to be greater than 96 %, which is particularly remarkable, given

its essentially zero fluorescence quantum yield ($\Phi_f < 0.002$).

Such high EnT efficiencies are facilitated by the small donor-acceptor separations within the catenane structure ($\sim$ 3.5 Å). The crystal structures of the catenanes show that the van der Waals radii of the PDI and Ex[1]Box components overlap, such that molecular orbital overlap should allow EnT to proceed *via* the electron exchange Dexter mechanism,[42] which is likely the dominant mechanism. The documentation of ultrafast charge transfer (< 250 fs) between $\mathbf{ExBox}^{4+}$ and perylene[2] demonstrates that such a mechanism involving electron exchange is certainly feasible. Although Förster theory[43] predicts critical transfer radii (see Table 4) such that EnT should be quantitative within the catenanes, at a donor-acceptor separation of 3.5 Å the point dipole approximation of Föster theory breaks down. However, a short-range multipolar description of EnT could, potentially, also account for the observed rate. Such an approach has been previously used to describe EnT within natural photosynthetic systems.[44]

Subsequent relaxation of the excited PDI components was further monitored. fsTA reveals that ^{1}*PDI is fully evolved within 1 ps for all ExCats (Figures 6, S22-S24). In both $\mathbf{ExCat}^{6+}$ and $\mathbf{TExCat}^{+6}$, the ground state bleach (445-580 nm), stimulated emission (575-630 nm), and excited state absorption features, in both visible and NIR regions, all decay with the same time constants as determined by a global fit to all of these features (see Figure S22-S23), which is in good agreement with the fluorescence lifetimes determined by TCSPS. ^{1}*PDI decays to the ground state mainly *via* fluorescence with a time constant of $\tau_{eff} = 5.85 \pm 0.03$ ns, for $ExCat^{6+}$ and $\tau_{eff} = 6.63 \pm 0.03$ ns for $\mathbf{TExCat}^{6+}$.

$\mathbf{SeExCat}^{6+}$, once again, displayed very different behavior. Upon excitation, we immediately observe the ^{1}*PDI spectrum. The stimulated emission and excited state absorption bands decay very quickly (fsTA, $\tau_{eff} = 1.56 \pm 0.04$ ns), while the PDI ground state bleach at approximately 530 nm remains throughout the experimental window. The higher energy PDI bleaches also remain, but rise with a similar time constant (global fitting, Figure S24) from the formation of a positive overlapping absorption corresponding to ^{3}*PDI, characterized[45]

by peak maxima at 485, 514, and 576 nm.

$$\frac{1}{\tau_{eff}} = \frac{1}{\tau_f} + \frac{1}{\tau_{ISC}} \tag{5}$$

Assuming $\tau_f = 3.7$ ns for ^{1}*PDI (taken from the fsTA analysis of the inclusion complex,[46] **PDI-E1⊂CB[8]**, Figures S29-S30), τ_{ISC} may be calculated using Equation 5, yielding $\tau_{ISC} \approx 2.7$ ns. TCSPC recorded a ^{1}*PDI lifetime of $\tau_{eff} = 1.75$ ns (Figure S36), which is in good agreement with fsTA, while Φ_f is heavily quenched (0.18) relative to **ExCat**$^{6+}$ and **TExCat**$^{6+}$ (0.90 and 0.77, respectively). The value of $\tau_f = 3.7$ ns for **PDI-E1⊂CB[8]** is similar to that of destacked PDIs measured in organic media,[47] indicating that the polarity of the **CB[8]** cavity is similar to that of organic solvents. However, as the cavities of the Ex^{1}Boxes are smaller than that of **CB[8]**, the microenvironments of their respective cavities are likely to be different. Therefore, one may also approximate the fluorescence lifetime of **SeExCat**$^{6+}$ as $\tau_f \approx 6$ ns (similar to that of **ExCat**$^{6+}$), which yields a value of $\tau_{ISC} \approx 2.1$ ns. Comparison of the ^{1}*PDI relaxation dynamics upon direct excitation ($\lambda_{ex} = 540$ nm) reveals similar behavior to that observed upon indirect excitation (Figures S25-S28).

SeExCat^{6+} was further investigated by nsTA and transient continuous wave electron paramagnetic resonance (TCW-EPR) to probe ^{3}*PDI. nsTA revealed a short triplet lifetime of $\tau_{eff} = 5.28 \pm 0.03$ μs in oxygenated solution at room temperature (Figures S33-S34), while TCW-EPR (85 K, Figure S39) shows the characteristic emission(e)-absorption(a) polarization pattern, e,e,e,a,a,a, for ^{3}*PDI formed *via* SO-ISC.[48] As such, **SeExCat**$^{6+}$ represents non-covalent method to generate the triplet state of a large, monomeric, aromatic chromophore in high yield in aqueous media *via* the external heavy atom effect, where El Sayed's selection rules formally forbid ^{1}*T(π-π*) $\leftarrow$ ^{1}*S(π-π*) SO-ISC.

Conclusion

Our work illustrates how extending components may be used to tune the light-harvesting antenna properties of Ex^1Boxes to cover a significant portion of the solar spectrum and generate a high energy, singlet state PDI in quantitative yield *via* energy transfer. As such, the alteration of the chemical environment of extended bipyridiniums allows for the tailored design of a family of organic, optoelectronic materials, exhibiting excellent electron accumulation properties, capable of incrementally accepting and stabilizing up to six electrons with tuneable redox potentials. Such properties afford potential for these materials in light-harvesting and catalytic applications, ranging from multi-electron catalytic processes, such as water splitting, to organic synthetic photocatalysis in water. Our work has also expanded our understanding of the excited state behavior of Ex^1Boxes, illustrating their phosphorescence properties.

A drawback is that upon tuning the HOMO-LUMO gap of ExBIPY^{2+}s using heavy atoms, energy is lost in the excited state PDI upon conversion to the triplet state. This could be circumvented by using fused heterocycle extending components as an alternative means to achieving solar spectrum coverage outside the presented range. Nevertheless, the ability of **SeExCat**$^{6+}$ to efficiently access PDI triplet states in high triplet quantum yields could find utility in triplet photosensitizing applications[49] in both aqueous and organic media. **SeExCat**$^{6+}$ also demonstrates how the design element of the ExCats allows for highly efficient EnT from an essentially nonfluorescent antenna.

The mono and higher-order functionalization of Ex^1Boxes[50] and PDIs[13] may also allow for the synthesis of novel ExCat derivatives capable of incorporating extra chromophores for additional electronic function and of surface attachment *via* multiple chemistries.

Acknowledgement

S.T.J.R. thanks the Cambridge Home and European Scholarship Scheme and the Robert

Gardiner memorial scholarship. S.T.J.R., A.F. and O.A.S. thank the ERC starting investigator grant ASPiRe (project no. 240629) and the EPSRC (reference no. EP/G060649/1). Femtosecond and nanosecond spectroscopy (R.M.Y.), EPR spectroscopy (M.D.K.) and phosphorescence spectroscopy (Y.W.) were supported as part of the ANSER Center, an Energy Frontier Research Center funded by the U.S. Department of Energy, Office of Science, Office of Basic Energy Sciences under award no. DE-SC0001059. J.F.S., J.J.H., N.H., N.A.V. and E.D.J. acknowledge the Joint Center of Excellence in Integrated Nano-Systems (JCIN) between KACST and Northwestern University (Project 34-946) for their continued financial support. E.J.D. acknowledges NSF and Ryan fellowships. A.H. and W.M.N. thank the COST Action CM1005 "Supramolecular Chemistry in Water" and the DFG (grant NA-686/5) for financial support. The authors also thank Charlotte L. Stern and Dr. Amy A. Sarjeant for helpful discussions and Mr. Michael J. Byrne for his artistic contribution.

Supporting Information Available

Detailed of synthetic procedures and characterization (NMR, HRMS) data for all new compounds, crystallographic characterization for **TExBox·4PF$_6$**, **SeExBox·4PF$_6$**, **ExCat·6PF$_6$** and **SeExCat·6PF$_6$**, additional fsTA, nsTA, TCW-EPR, TCSPC, CV, ITC, electronic absorption, fluorescence and phosphorescence characterization data. This material is available free of charge via the Internet at `http://pubs.acs.org/`.

References

(1) Barnes, J. C.; Juríček, M.; Strutt, N. L.; Frasconi, M.; Sampath, S.; Giesener, M. A.; McGrier, P. L.; Bruns, C. J.; Stern, C. L.; Sarjeant, A. A.; Stoddart, J. F. *J. Am. Chem. Soc.* **2013**, *135*, 183–192.

(2) Young, R. M.; Dyar, S. M.; Barnes, J. C.; Juríček, M.; Stoddart, J. F.; Co, D. T.; Wasielewski, M. R. *J. Phys. Chem. A*. **2013**, *117*, 12438–12448.

(3) Dyar, S. M.; Barnes, J. C.; Juríček, M.; Stoddart, J. F.; Co, D. T.; Young, R. M.; Wasielewski, M. R. *Angew. Chem. Int. Ed.* **2014**, *53*, 5371–5375.

(4) Ryan, S. T. J.; Del Barrio, J.; Ghosh, I.; Biedermann, F.; Lazar, A. I.; Lan, Y.; Coulston, R. J.; Nau, W. M.; Scherman, O. A. *J. Am. Chem. Soc.* **2014**, *136*, 9053–9060.

(5) Pullerits, T.; Sundström, V. *Acc. Chem. Res.* **1996**, *29*, 381–389.

(6) McDermott, G.; Prince, S. M.; Freer, A. A.; Hawthornthwaite-Lawless, A. M.; Papiz, M.; Cogdell, R. J.; Isaacs, N. *Nature* **1995**, *374*, 517–521.

(7) Kühlbrandt, W.; Wang, D. N. *Nature* **1991**, *350*, 130–134.

(8) Kühlbrandt, W.; Wang, D. N.; Fujiyoshi, Y. *Nature* **1994**, *367*, 614–621.

(9) Kühlbrandt, W. *Nature* **1995**, *374*, 497–498.

(10) Barber, J., Ed. *Primary processes of photosynthesis*; Elsevier Scientific Pub. Co.: Amsterdam; New York, 1977.

(11) Stoddart, J. F. *Angew. Chem. Int. Ed.* **2014**, *53*, 11102–11104.

(12) Coskun, A.; Spruell, J. M.; Barin, G.; Dichtel, W. R.; Flood, A. H.; Botros, Y. Y.; Stoddart, J. F. *Chem. Soc. Rev.* **2012**, *41*, 4827–4859.

(13) Huang, C.; Barlow, S.; Marder, S. R. *J. Org. Chem.* **2011**, *76*, 2386–2407.

(14) Zhan, X.; Facchetti, A.; Barlow, S.; Marks, T. J.; Ratner, M. A.; Wasielewski, M. R.; Marder, S. R. *Adv. Mater.* **2011**, *23*, 268–284.

(15) Li, C.; Liu, M.; Pschirer, N. G.; Baumgarten, M.; Müllen, K. *Chem. Rev.* **2010**, *110*, 6817–6855.

(16) Ghosh, I.; Ghosh, T.; Bardagi, J. I.; König, B. *Science* **2014**, *346*, 725–728.

(17) Ronconi, F.; Syrgiannis, Z.; Bonasera, A.; Prato, M.; Argazzi, R.; Caramori, S.; Cristino, V.; Bignozzi, C. A. *J. Am. Chem. Soc.* **2015**, *137*, 4630–4633.

(18) Weingarten, A. S.; Kazantsev, R. V.; Palmer, L. C.; McClendon, M.; Koltonow, A. R.; Samuel, A. P. S.; Kiebala, D. J.; Wasielewski, M. R.; Stupp, S. I. *Nat. Chem.* **2014**, *6*, 964–970.

(19) Quaschning, V. *Renewable Energy and Climate Change*; John Wiley & Sons, Ltd, 2010; pp 70–86.

(20) Takahashi, K.; Nihira, T.; Akiyama, K.; Ikegami, Y.; Fukuyo, E. *J. Chem. Soc., Chem. Commun.* **1992**, 620–622.

(21) Sauvage, J.-P., Dietrich-Buchecker, C., Eds. *Molecular catenanes, rotaxanes and knots : a journey through the world of molecular topology*; Wiley-VCH: Weinheim; Chichester, 1999.

(22) Wang, W.; Wang, L.; Palmer, B. J.; Exarhos, G. J.; Li, A. D. Q. *J. Am. Chem. Soc.* **2006**, *128*, 11150–11159.

(23) Hay, A. S. *J. Org. Chem.* **1962**, *27*, 3320–3321.

(24) Fomina, L.; Vazquez, B.; Tkatchouk, E.; Fomine, S. *Tetrahedron* **2002**, *58*, 6741–6747.

(25) Fang, L.; Basu, S.; Sue, C.-H.; Fahrenbach, A. C.; Stoddart, J. F. *J. Am. Chem. Soc.* **2011**, *133*, 396–399.

(26) Attempts to grow single crystals of $\mathbf{TExCat}^{6+}$ suitable for X–ray diffraction have, thus far, been unsuccessful.

(27) Kaifer, A. E.; Gómez-Kaifer, M. *Supramolecular electrochemistry [electronic resource]*; Wiley-VCH: Weinheim; New York, 1999.

(28) Arachchige, S. M.; Brown, J. R.; Chang, E.; Jain, A.; Zigler, D. F.; Rangan, K.; Brewer, K. J. *Inorg. Chem.* **2009**, *48*, 1989–2000.

(29) Oliva, M. M.; Casado, J.; Hennrich, G.; Navarrete, J. T. L. *J. Phys. Chem. B.* **2006**, *110*, 19198–19206.

(30) Konduri, R.; Ye, H.; MacDonnell, F. M.; Serroni, S.; Campagna, S.; Rajeshwar, K. *Angew. Chem. Int. Ed.* **2002**, *41*, 3185–3187.

(31) Klán, P. *Photochemistry of organic compounds [electronic resource] : from concepts to practice*; Wiley: Chichester, U.K, 2009.

(32) An impurity was observed in our $\mathbf{MSeV}^{2+}$ sample, the excited state decay of which, (τ_{eff} = 108 ± 1 ps) was accounted for in our data analysis (Figures S13, S16).

(33) Koziar, J. C.; Cowan, D. O. *Acc. Chem. Res.* **1978**, *11*, 334–341.

(34) Albert, W. *Z. Phys. Chem* **1982**, *1133*, 93–98.

(35) Fukuzumi, S.; Ohkubo, K.; Suenobu, T.; Kato, K.; Fujitsuka, M.; Ito, O. *J. Am. Chem. Soc.* **2001**, *123*, 8459–8467.

(36) El-Sayed, M. A. *J. Chem. Phys.* **1974**, *60*, 4502–4507.

(37) Klán, P. *Photochemistry of organic compounds [electronic resource] : from concepts to practice*; Wiley: Chichester, U.K, 2009.

(38) An impurity was observed in our $\mathbf{SeExBox}^{4+}$ sample, the excited state decay of which, (τ_{eff} = 197 ± 7 ps) was accounted for in our data analysis.

(39) An, Z.; Zheng, C.; Tao, Y.; Chen, R.; Shi, H.; Chen, T.; Wang, Z.; Li, H.; Deng, R.; Liu, X.; Huang, W. *Nat. Mater.* **2015**, *14*, 1476–4660.

(40) Baldo, M. A.; O'Brien, D. F.; You, Y.; Shoustikov, A.; Sibley, S.; Thompson, M. E.; Forrest, S. R. *Nat. Chem.* **1998**, *395*, 151–154.

(41) Lakowicz, J. R. *Principles of fluorescence spectroscopy*, 3rd ed.; Springer: New York, 2006.

(42) Dexter, D. L. *J. Chem. Phys.* **1953**, *21*, 836–850.

(43) Förster, T. *Annalen der Physik* **1948**, *437*, 55–75.

(44) Chang, J. C. *J. Chem. Phys.* **1977**, *67*, 3901–3909.

(45) Lefler, K. M.; Brown, K. E.; Salamant, W. A.; Dyar, S. M.; Knowles, K. E.; Wasielewski, M. R. *J. Phys. Chem. A*. **2013**, *117*, 10333–10345.

(46) Biedermann, F.; Elmalem, E.; Ghosh, I.; Nau, W. M.; Scherman, O. A. *Angew. Chem. Int. Ed.* **2012**, *51*, 7739–7743.

(47) Ford, W. E.; Kamat, P. V. *J. Phys. Chem.* **1987**, *91*, 6373–6380.

(48) Carmieli, R.; Zeidan, T. A.; Kelley, R. F.; Mi, Q.; Lewis, F. D.; Wasielewski, M. R. *J. Phys. Chem. A*. **2009**, *113*, 4691–4700.

(49) Zhao, J.; Wu, W.; Sun, J.; Guo, S. *Chem. Soc. Rev.* **2013**, *42*, 5323–5351.

(50) Klajn, R.; Olson, M. A.; Wesson, P. J.; Fang, L.; Coskun, A.; Trabolsi, A.; Soh, S.; Stoddart, J. F.; Grzybowski, B. A. *Nat. Chem.* **2009**, *1*, 733–738.

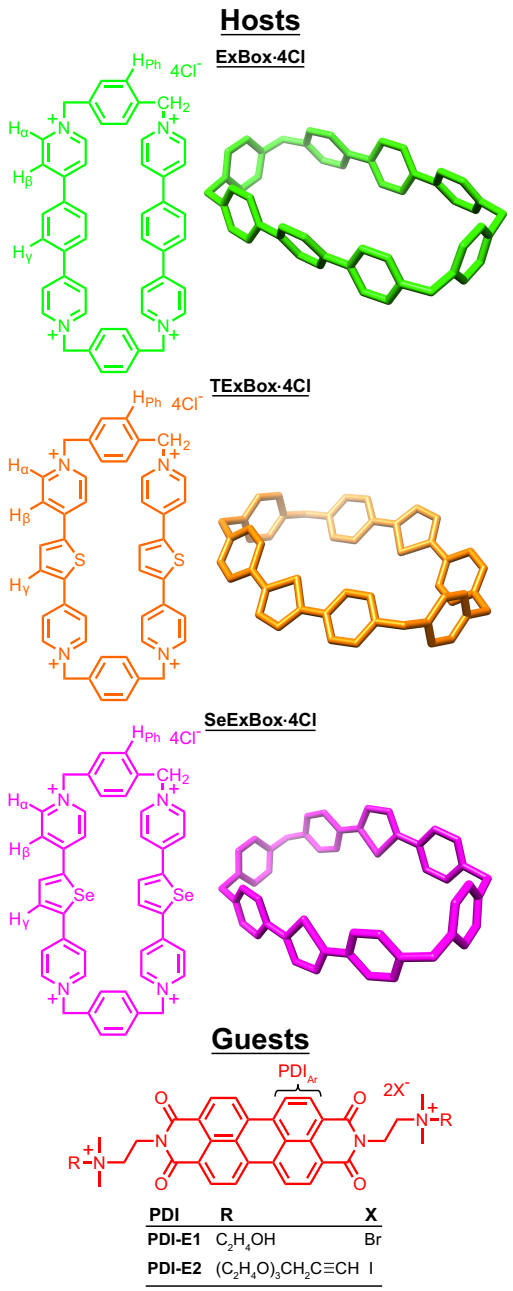

Figure 1: Structural formulae and X-ray crystal structures of **ExBox·4Cl**,[1] **TExBox·4Cl**, **SeExBox·4Cl** and the PDIs. PF_6^- counterions and solvent molecules have been removed for clarity.

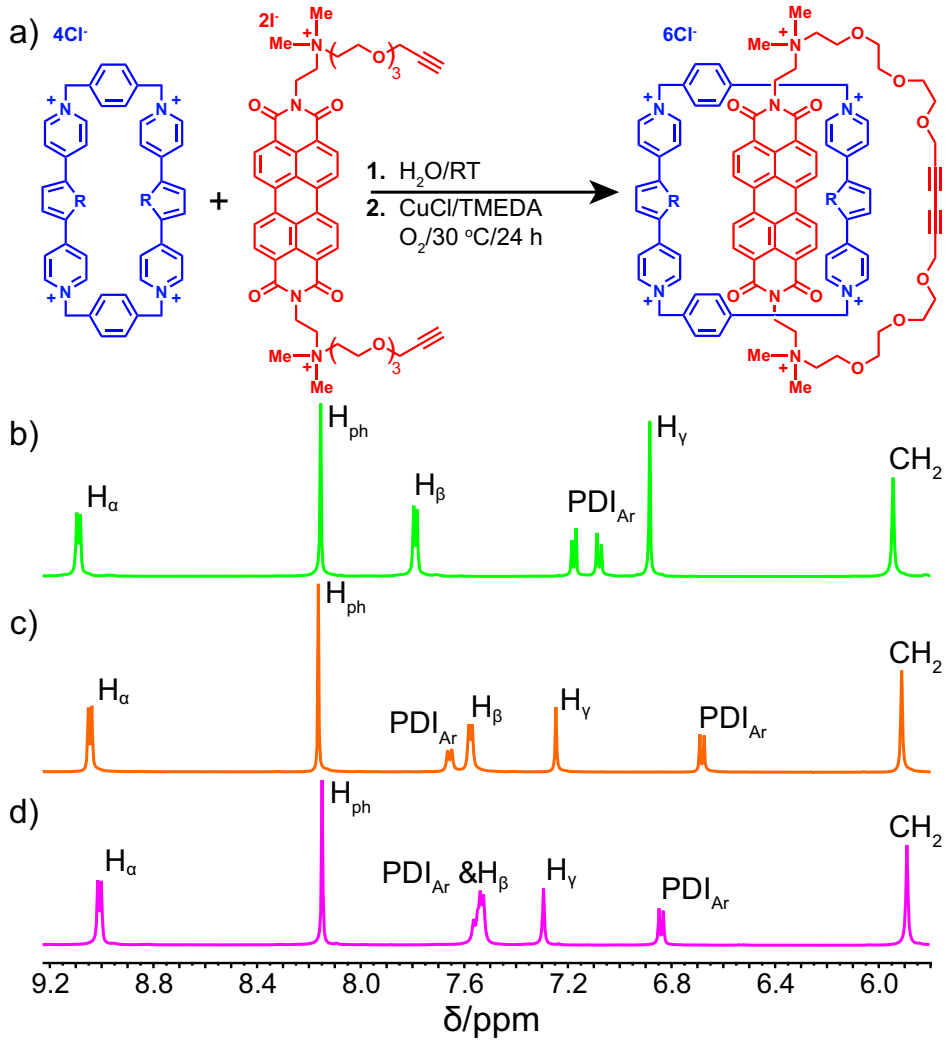

Figure 2: (**a**) Procedure for ExCat synthesis. R = $\mathbf{C_2H_2}$ ($\mathbf{ExBox}^{4+}$/$\mathbf{ExCat}^{6+}$), **S** ($\mathbf{TExBox}^{4+}$/$\mathbf{TExCat}^{6+}$) and **Se** ($\mathbf{SeExBox}^{4+}$/$\mathbf{SeExCat}^{6+}$). ^{1}H NMR spectra (D_2O, 1 mM, Cl^- counterions) of (**b**) $\mathbf{ExCat}^{6+}$, (**c**) $\mathbf{TExCat}^{6+}$ and (**d**) $\mathbf{SeExCat}^{6+}$.

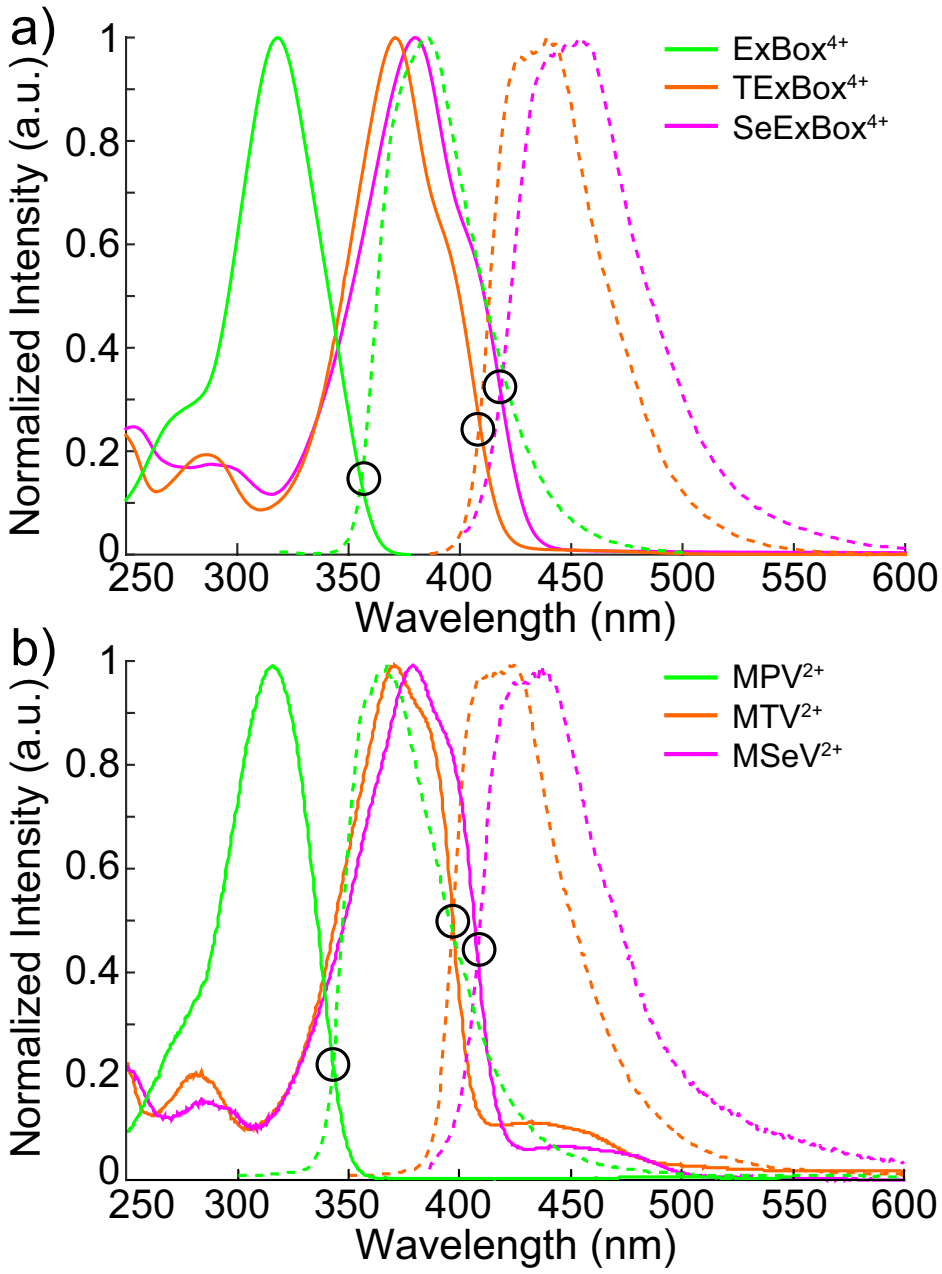

Figure 3: (**a**) Normalized electronic absorption (solid line) and fluorescence emission (dashed lines) spectra of $\mathbf{ExBox}^{4+}$ (λ_{ex} = 319 nm), $\mathbf{TExBox}^{4+}$ (λ_{ex} = 371 nm) and $\mathbf{SeExBox}^{4+}$ (λ_{ex} = 380 nm). (**b**) Normalized electronic absorption (solid line) and fluorescence emission (dashed lines) spectra of $\mathbf{MPV}^{2+}$ (λ_{ex} = 315 nm), $\mathbf{MTV}^{2+}$ (λ_{ex} = 378 nm) and $\mathbf{MSeV}^{2+}$ (λ_{ex} = 378 nm). All measurements were performed in water with Cl^- counterions. Black circles indicate the cross over points of absorption and emission spectra, which represent excited state singlet energies.

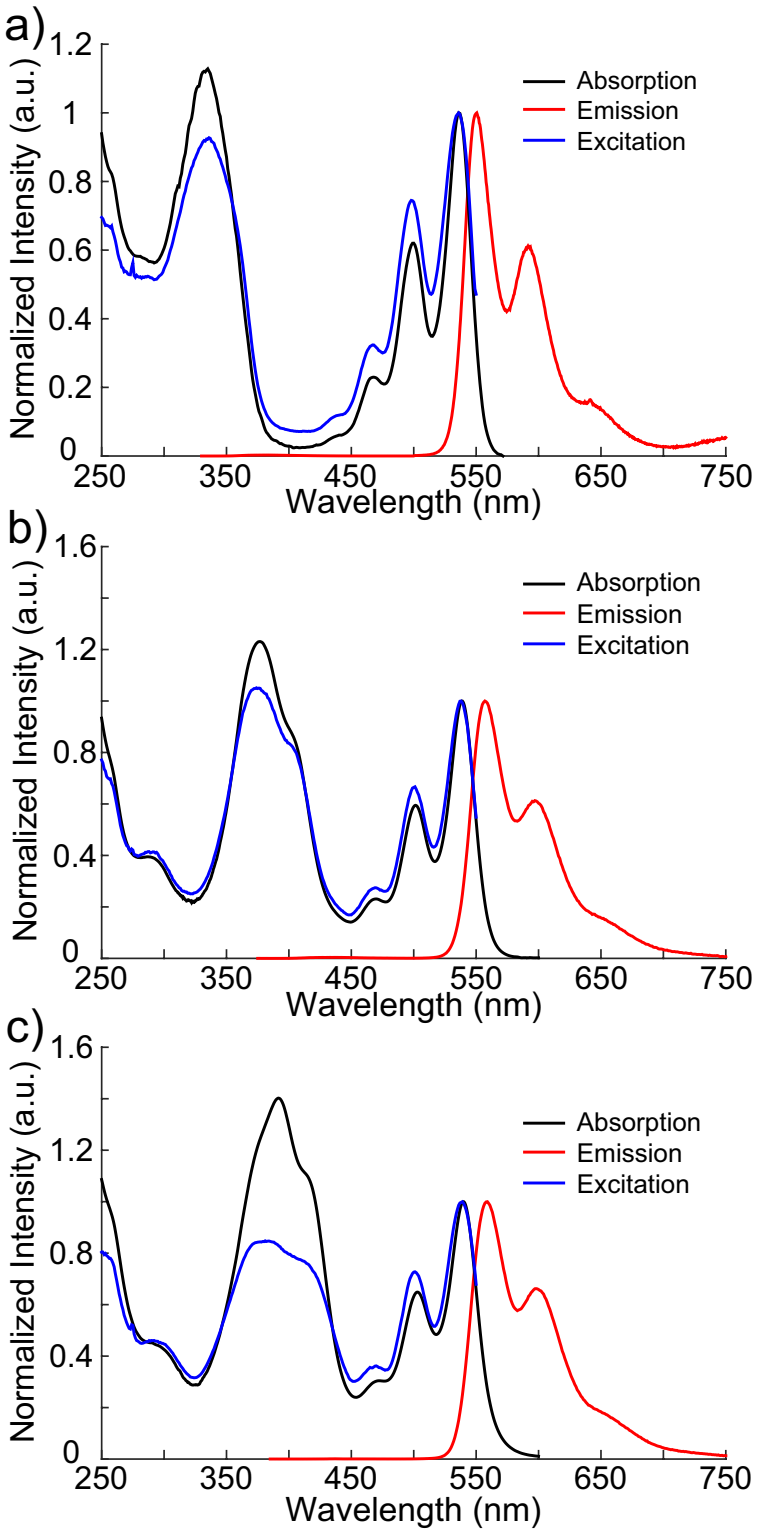

Figure 4: Normalized absorption, excitation (λ_{mon} = 550 nm) and emission spectra of (**a**) **ExCat**$^{6+}$ (λ_{ex} = 320 nm), (**b**) **TExCat**$^{6+}$ (λ_{ex} = 377 nm), and (**c**) **SeExCat**$^{6+}$ (λ_{ex} = 392 nm). All measurements were performed in water with Cl^- counterions.

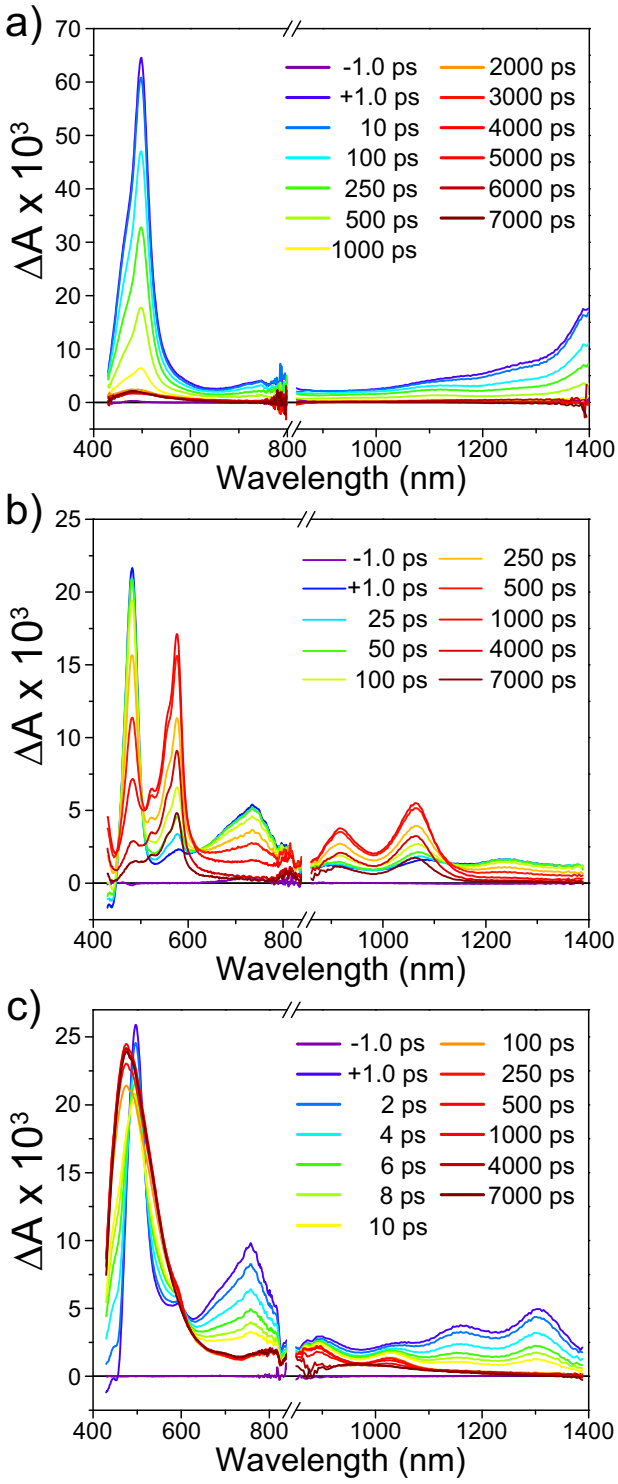

Figure 5: Combined visible and near-infrared femtosecond transient absorption spectra of (**a**) **ExBox**$^{4+}$ (λ_{ex} = 330 nm, 0.4 μJ pulse^{-1}), (**b**) **TExBox**$^{4+}$ (λ_{ex} = 414 nm, 1.0 μJ pulse^{-1}) and (**c**) **SeExBox**$^{4+}$ (λ_{ex} = 414 nm, 1.0 μJ pulse^{-1}). Relative amplitudes on either side of the vertical break are arbitrary. All measurements were performed in water with Cl^- counterions.

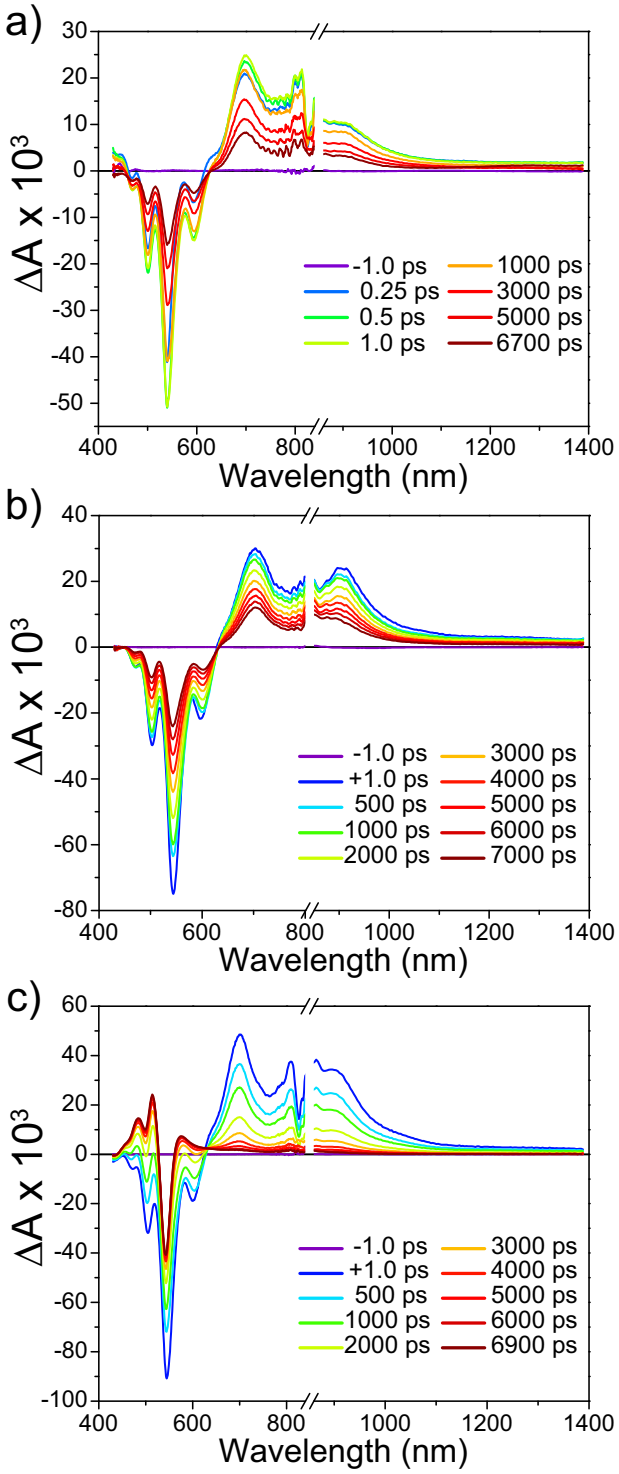

Figure 6: Combined visible and near-infrared femtosecond transient absorption spectra of (**a**) **ExCat**$^{6+}$ (λ_{ex} = 330 nm, 0.4 μJ pulse^{-1}), (**b**) **TExCat**$^{6+}$ (λ_{ex} = 414 nm, 1.0 μJ pulse^{-1}) and (**c**) **SeExCat**$^{6+}$ (λ_{ex} = 414 nm, 1.0 μJ pulse^{-1}). Relative amplitudes on either side of the vertical break are arbitrary. All measurements were performed in water with Cl^- counterions.

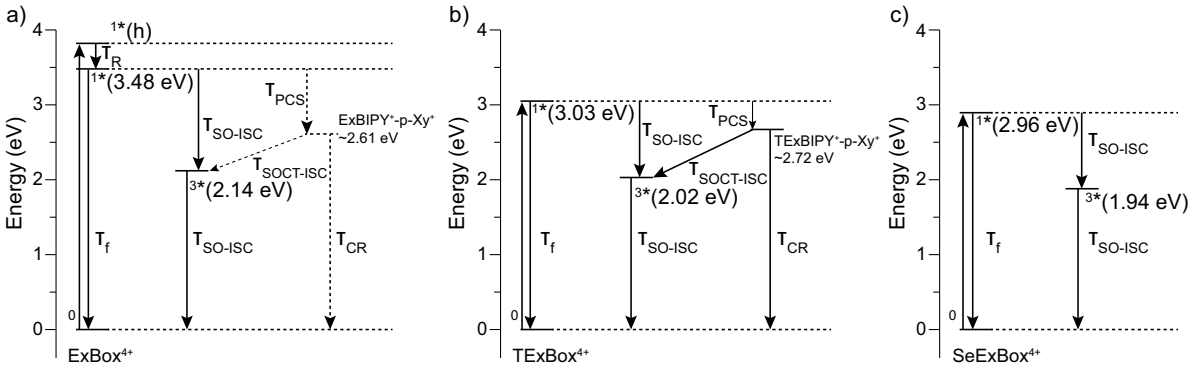

Scheme 1: Energetics and excited state relaxation dynamics for fluorescence (τ_f), spin-orbit intersystem crossing (τ_{SO-ISC}), photoinduced charge separation (τ_{PCS}), spin-orbit charge transfer intersystem crossing ($\tau_{SOCT-ISC}$) and charge recombination (τ_{CR}) in (**a**) **ExBox**$^{4+}$, (**b**) **TExBox**$^{4+}$ and (**c**) **SeExBox**$^{4+}$. Dashed lines indicate hypothesized processes. All time constants are described in the text and Table 3.

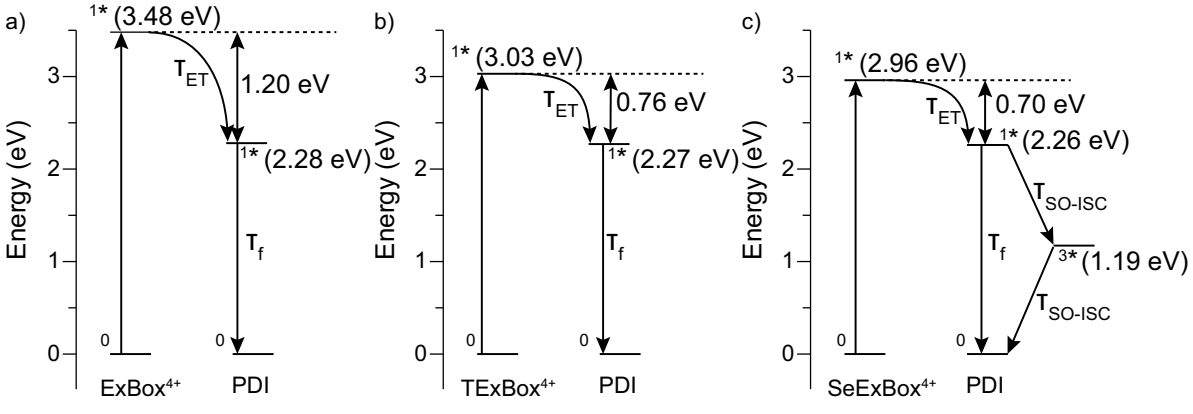

Scheme 2: Energetics and dynamics for photodriven energy transfer (τ_{EnT}), fluorescence (τ_f) and spin-orbit intersystem crossing (τ_{SO-ISC}) in (**a**) **ExCat**$^{6+}$, (**b**) **TExCat**$^{6+}$ and (**c**) **SeExCat**$^{6+}$. ^{1*}T PDI energy from ref.[47] All time constants are described in the text and Table 4.

Table 1: Electrochemical half-wave redox potentials of the MExVs, Ex[1]Boxes and ExCats in Me_2SO

Compound	1^{st} $E_{1/2}$ (V)[a]	2^{nd} $E_{1/2}$ (V)[a]	3^{rd} $E_{1/2}$ (V)[a]
MPV^{2+}	-0.82	–	–
MTV^{2+}	-0.74	-0.85	–
MSeV^{2+}	-0.64	-0.76	–
ExBox^{4+}	-0.82	–	–
TExBox^{4+}	-0.49	-0.63	–
SeExBox^{4+}	-0.34	-0.46	–
ExCat^{6+}	-0.25	-0.48	-0.78
TExCat^{6+}	-0.21	-0.45	-0.68
SeExCat^{6+}	-0.21	-0.42	-0.61
PDI-E1	-0.34	-0.51	–

[a] Determined by cyclic voltammetry. A glassy carbon working electrode, an Ag/AgCl reference electrode and a platinum counter electrode were used to characterize 1 mM Me_2SO solutions of the hexfluorophosphate salts of the analytes at 298 K, with 0.1 M $TBAPF_6$ serving as the supporting electrolyte at a scan rate of 50 mVs^{-1}. Due to the closely overlapping peaks of **SeExBox**$^{4+}$ and **MSeV**$^{2+}$, an error of ± 0.2 V is estimated for their half-wave redox potentials.

Table 2: Steady-state photophysical properties of the Ex[1]Boxes and MExVs

Compound	Electronic Absorption Maximum (nm)	Fluorescence Emission Maximum (nm)[a]	Fluorescence Quantum Yield (Φ_f)[b]	Singlet Energy (eV)[c]	Triplet Energy (eV)[d]
ExBox^{4+}	318	386	0.21	3.48	2.14
MPV^{2+}	314	371	0.68	3.59	–
TExBox^{4+}	371	439	0.37	3.03	2.02
MTV^{2+}	370	416	0.77	3.11	–
SeExBox^{4+}	378	454	0.0027	2.96	1.94
MSeV^{2+}	380	434	0.0017	3.02	–

[a] Excitation wavelengths (λ_{ex}) used for each ExTC/MExV corresponded to its electronic absorption maximum as detailed in the first column. [b] See ESI for conditions used for fluorescence quantum yield determination. [c] Determined by the intersection of the normalized electronic absorption and fluorescence emission spectra. [d] Determined by the peak maxima of the phosphorescence emission spectra. Triplet energies were not obtained for MExVs.

Table 3: Time constants (τ, ps) for the decay of the singlet excited states of the MExVs and Ex^{1}Boxes, as measured by femtosecond transient absorption spectroscopy in water

Compound	^{1}*Singlet(h)[a]	^{1}*Singlet	Decay Mechanism[b]
ExBox^{4+}	73 ± 10	413 ± 7	see text
MPV^{2+}	96 ± 1	1330 ± 15	Fluorescence, IC
TExBox^{4+}	–	447 ± 4	Fluorescence, PCS[c]
MTV^{2+}	71 ± 2	1080 ± 8	Fluorescence, IC
SeExBox^{4+}	–	6.6 ± 0.1	SO-ISC
MSeV^{2+}	–	5.1 ± 0.1	SO-ISC

[a] "(h)" indicates a vibrationally excited state. [b] IC = internal conversion, SO-ISC = spin-orbit intersystem crossing. [c] PCS = photoinduced charge separation. Charge recombination occurs with a lifetime of 2850 ps.

Table 4: Photophysical properties of the ExCats in water

Compound	Förster Distance (Å)[a]	Fluorescence Quantum Yield[b]	Fluorescence Lifetime (τ, ns)[c]	Excitation Window (nm)[d]	PDI ^{1}*Singlet lifetime (τ, ns)[e]
ExCat^{6+}	26.3[f]	0.90	6.30	293 - 360 (335)	5.85 ± 0.03
TExCat^{6+}	37.9	0.76	6.45	351 - 414 (377)	6.63 ± 0.03
SeExCat^{6+}	18.2	0.18	1.75	355 - 430 (391)	1.56 ± 0.04

[a] Determined using the absorption spectrum of **PDI-E1**⊂CB[8] as an approximation for the disaggregated absorption spectrum of PDI in water and a κ^2 value of 2/3. [b] Determined by relative measurement with Rhodamine 6G in ethanol as fluorescence quantum yield standard ($\Phi_f = 0.95$). [c] Determined by TCSPC. Excitation wavelength (λ_{ex}) = 510 nm, monitored wavelength (λ_{mon}) = 550 nm, error ± 3%. [d] Defined as the FWHM of the ExTC ^{1}*← ^{0}S absorption peaks (absorption maxima are shown in parenthesis).
[e] Determined by fsTA. Indirect excitation (λ_{ex} = 330 nm for **ExCat**$^{6+}$; λ_{ex} = 414 nm for **TExCat**$^{6+}$ and **SeExCat**$^{6+}$). [f] from ref.[4]

Graphical TOC Entry